buildings

MDPI

Article

Hilbert-Huang Transform-Based Seismic Intensity Parameters for Performance-Based Design of RC-Framed Structures

Magdalini Tyrtaiou [1], Anaxagoras Elenas [1,*], Ioannis Andreadis [2] and Lazaros Vasiliadis [1]

[1] Department of Civil Engineering, Institute of Structural Statics and Dynamics, Democritus University of Thrace, 67100 Xanthi, Greece
[2] Laboratory of Electronics, Department of Electrical and Computer Engineering, Democritus University of Thrace, 67100 Xanthi, Greece
* Correspondence: elenas@civil.duth.gr; Tel.: +30-2541-079-626

Abstract: This study aims to develop the optimal artificial neural networks (ANNs) capable of estimating the seismic damage of reinforced concrete (RC)-framed structures by considering several seismic intensity parameters based on the Hilbert–Huang Transform (HHT) analysis. The selected architecture of ANN is the multi-layer feedforward perceptron (MFP) network. The values of the HHT-based parameters were calculated for a set of seismic excitations, and a combination of five to twenty parameters was performed to develop input datasets. The output data were the structural damage expressed by the Park and Ang overall damage index ($DI_{PA,global}$). The potential contribution of nine training algorithms to developing the most effective MFP was also investigated. The results confirm that the evolved MFP networks, utilizing the employed parameters, provide an accurate estimation of the target output of $DI_{PA,global}$. As a result, the developed MFPs can constitute a reliable computational intelligence approach for determining the seismic damage induced on structures and, thus, a powerful tool for the scientific community for the performance-based design of buildings.

Keywords: seismic intensity parameters; Hilbert–Huang Transform (HHT); artificial neural networks; Park and Ang damage index; damage index assessment

check for updates

Citation: Tyrtaiou, M.; Elenas, A.; Andreadis, I.; Vasiliadis, L. Hilbert-Huang Transform-Based Seismic Intensity Parameters for Performance-Based Design of RC-Framed Structures. *Buildings* **2022**, *12*, 1301. https://doi.org/10.3390/buildings12091301

Academic Editor: Asimina Athanatopoulou-Kyriakou

Received: 28 July 2022
Accepted: 22 August 2022
Published: 25 August 2022

1. Introduction

The fast, comprehensive, and accurate coverage of existing and planned structures' seismic hazards is a central task in earthquake engineering. The results of the seismic hazard estimation serve as a basis for preparing disaster plans and as a tool for determining premiums in the insurance industry and the damage forecast. It is well known that seismic intensity parameters have been widely used to express the damage potential of earthquakes [1,2]. Furthermore, structural damage indices have been used to express the postseismic damage status of buildings [1–11]. Several studies verified the correlation between seismic intensity parameters and seismic damage [1,2,6–9]. However, no explicit formula or algorithm exists for directly evaluating damage indices from seismic intensity parameters. Therefore, knowing the seismic intensity parameters, statistical and artificial intelligence techniques have been used to estimate the postseismic damage status of buildings, expressed by structural damage indices. Such established techniques in earthquake engineering are multilinear regression analysis and artificial intelligence procedures, such as ANNs [3–6,9,12–16]. Additionally, damage indices are essential quantities in performance-based design [17–21].

On the other hand, the HHT procedure is appropriate for processing nonlinear and nonstationary signals such as seismic excitation records [22–26]. Thus, new HHT-based seismic intensity parameters have been developed recently, considering the frequency-time history of seismic accelerograms. This study uses the multi-layer feedforward perceptron (MFP) ANN framework to evaluate the structural damage index used in recently developed HHT-based seismic intensity quantities for the first time [10,11]. The result values of the used structural damage index provided by the ANNs are compared with the corresponding results provided by nonlinear dynamic analyses, which have been considered exact results. The quality of the ANNs' results is confirmed by the performance evaluation parameters mean squared error (MSE) and R correlation coefficient.

The seismic intensity measures can be classified into peak, spectral, and energy parameters. Generally, these conventional parameters ignore the frequency-time history of the seismic excitation, which is their main disadvantage in this context. The HHT is a procedure for processing nonlinear and nonstationary signals, such as seismic excitation records, which provide the frequency-time history of the seismic time histories [22–26]. HHT-based parameters overcome the disadvantage of the conventional intensity parameters mentioned above. In contrast to a large number of conventional seismic intensity parameters, only a relatively small number of HHT-based parameters have been defined and applied in seismic engineering. The present study covers this gap; thus, 40 HHT-based recently defined seismic intensity parameters have been considered [10,11].

The 40 HHT-based, recently developed seismic intensity parameters [10,11] used in this study have not yet been investigated in combination with ANNs. However, these parameters provided promising results in combination with statistical methods (correlation studies, multilinear regression analysis) [10,11]. The 40 used seismic intensity parameters are investigated in this study for the first time combined with ANNs procedures to determine their effectiveness in predicting the postseismic damage status of a building in terms of a structural damage index.

2. Methods

2.1. Hilbert-Huang Transform (HHT) Analysis

The Hilbert–Huang transform (HHT) is an innovative signal processing technique suitable for nonstationary and nonlinear signals [22]. HHT uses an adaptive basis derived from the data collected as the natural phenomenon unfolds over time. In contrast to other standard techniques for analyzing signals (e.g., wavelet analysis, Fourier transform), it assumes that signals are stationary, within the time window of observation at least, and are associated with no adaptive bases.

The HHT technique is a combination of two stages, namely, empirical mode decomposition (EMD) and Hilbert analysis (HA):

The empirical mode decomposition (EMD) decomposes complex signal data assuming that, at any given time, the signal consists of coexisting simple oscillatory modes of notably different frequencies, one superimposed on the other. In the end, the EMD algorithm manages to separate the data into locally non-overlapping time scale components, the intrinsic mode functions (IMF) with physical meaning, which follow specific conditions.

Hence, the initial signal $X(t)$ was decomposed into a sum of n IMFs $c_j(t)$ and a residual r_n which was either a monotonic function or a constant

$$X(t) = \sum_{J=1}^{n} c_j(t) + r_n\,(t) \tag{1}$$

After extracting the IMFs $c_j(t),\ j = 1, 2, \ldots, n$, of a signal, the Hilbert transform $y_j(t)$ was applied to each of them, as described in the following equation

$$y_j(t) = \frac{1}{\pi}\,P\int_{-\infty}^{\infty} \frac{c_j(\tau)}{t-\tau}\,d\tau, \tag{2}$$

where P denotes the Cauchy principal value of the integral.

The IMF $c_j(t)$ and the Hilbert transform $y_j(t)$ form an analytical signal $z_j(t)$ as follows:

$$z_j(t) = c_j(t) + iy_j(t) = a_j(t)e^{i\theta j(t)} \tag{3}$$

from which the amplitude $a_j(t)$ and the phase function $\theta_j(t)$ were defined.

$$a_j(t) = \sqrt{c_j^2(t) + y_j^2(t)} \quad \text{και} \quad \theta_j(t) = \arctan\left(\frac{y_j(t)}{c_j(t)}\right) \tag{4}$$

Furthermore, the instantaneous frequency was calculated from the phase function's first derivative.

$$\omega_j(t) = \frac{d\theta_j(t)}{dt} \tag{5}$$

Knowing the instantaneous frequencies and amplitudes of the IMFs, a frequency-time distribution of amplitude (energy) was designated as the "Hilbert Spectrum" (HS) and defined below as:

$$H(\omega, t) = Re\left[\sum_{j=1}^{n} a_j(t) e^{i \int \omega_j(t) dt}\right] \tag{6}$$

The calculation procedure of the two-step HHT algorithm is illustrated in Figure 1. The left-hand side of Figure 1 shows the procedure for using the empirical mode decomposition (sifting process) to define the IMFs, while the right-hand side shows the procedure to construct the Hilbert spectrum.

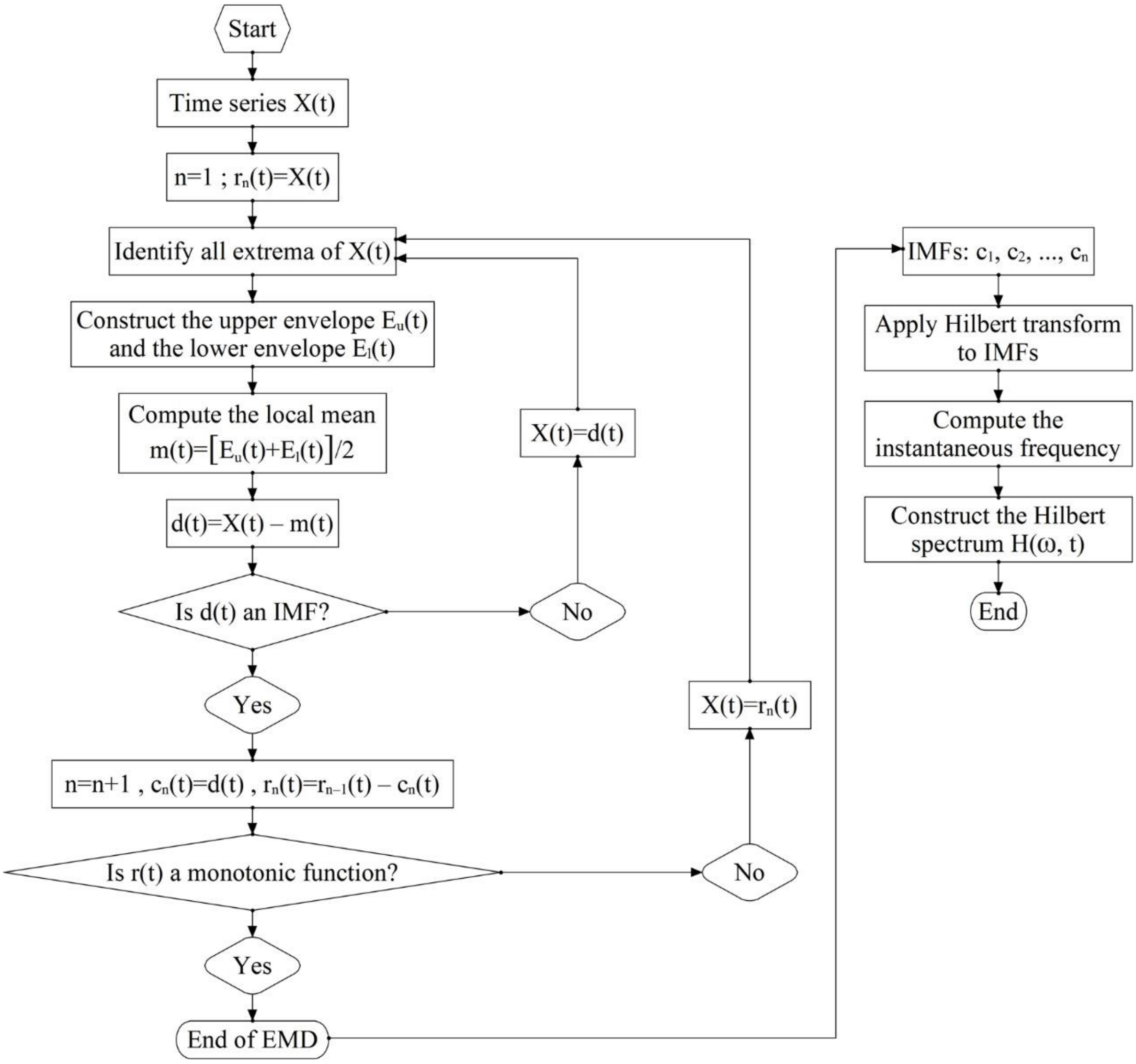

Figure 1. Flowchart of Hilbert–Huang Transform (HHT) Analysis.

2.2. HHT-Based Seismic Parameters

The study, through Hilbert spectra, of the inherent features of signals and their differences as the difference between their frequency content and the amplitude fluctuations across the time range, has led to the development of a number of new seismic intensity parameters, which have already been presented in the scientific literature [10,11].

After the evaluation of Hilbert spectra and their graphical representation, the connection between their geometrical features with the characteristics of the signals, the following forty seismic parameters were extracted and calculated for this research.

The first parameter was the volume $V_{1(HHT)}$ occupied by each spectrum, which represents the released energy during a seismic excitation and was calculated as

$$V_{1(HHT)} = \int_0^{f_{max}} \int_0^{t_{max}} a(f,t) \cdot df \cdot dt, \tag{7}$$

where $a(f,t)$ denotes the instantaneous amplitude, which corresponds to the instantaneous frequency f at a time equal to t, while f_{max} and t_{max} are the maximum instantaneous frequency calculated by the analytical signal and the total duration of the signal, respectively.

The upper surface of the defined volume $V_{1(HHT)}$ obtained from every Hilbert spectrum was the second seismic parameter and was described as

$$S_{1(HHT)} = \int_0^{f_{max}} \int_0^{t_{max}} \sqrt{1 + \left(\frac{da(f,\ t)}{df}\right)^2 + \left(\frac{da(f,t)}{dt}\right)^2} \cdot df \cdot dt \tag{8}$$

From the values of the instantaneous amplitude $\alpha(f,t)$ obtained from the analytical signal, the maximum, the mean values, and their difference were distinguished and considered additional parameters, which were described as

$$\begin{gathered} A_{1(max,HHT)} = max(\alpha(f,t)), \quad A_{1(mean,HHT)} = mean(\alpha(f,t)) \ \text{και} \\ A_{1(dif,HHT)} = A_{1(max,HHT)} - A_{1(mean,HHT)} \end{gathered} \tag{9}$$

Identifying that the magnitude and quantity of the maximum amplitude values of every signal are related to the destructive potential of excitation, a first limitation of the Hilbert spectrum was realized. Therefore, a parallel layer to the time-frequency one, which intersects the z-axis (axis of α amplitudes) of the Hilbert spectrum at the point of the $A_{1(mean,HHT)}$ value, was set (Figure 2). For the bounded Hilbert spectrum, the new volume $V_{1(Pos,HHT)}$, the volume over the parallel layer, and the new upper surface $S_{1(Pos,HHT)}$ of the spectrum were defined as two more parameters.

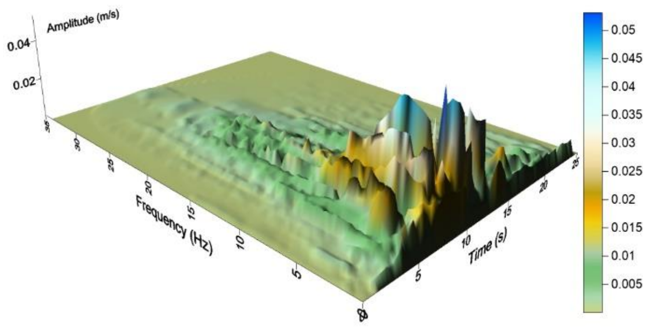

(**a**)

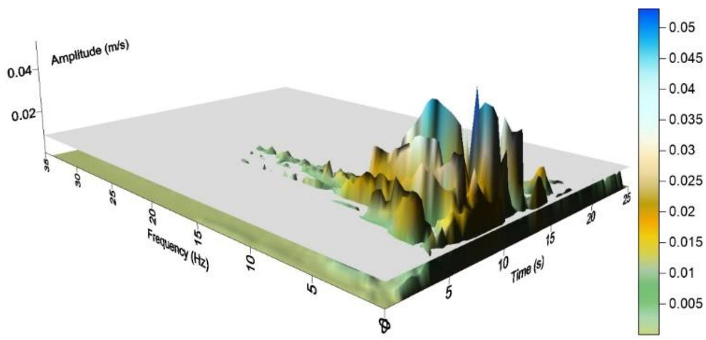

(**b**)

Figure 2. (**a**) Hilbert spectrum (HS) for a seismic excitation; (**b**) bounded HS with the layer that crosses the amplitude-axis of HS at $A_{mean,HHT}$.

The volumes $V_{1(HHT)}$ and $V_{1(Pos,HHT)}$ were divided by the corresponding values of surfaces $S_{1(HHT)}$ and $S_{1(Pos,HHT)}$, respectively, and so, the parameters $A_{1(HHT)}$ and $A_{1(Pos,HHT)}$ were calculated.

The seismic parameters $VA_{1(max,HHT)}$, $VA_{1(mean,HHT)}$, and $VA_{1(dif,HHT)}$ were set by the multiplication of the volume $V_{1(HHT)}$ with the maximum, minimum values of amplitude and their difference correspondingly.

Moreover, comparing the frequency content of a seismic excitation with the fundamental frequency of a structure is helpful in identifying possible resonance phenomena between the structure and soil vibration, which result in maximum values of the response forces. For this reason, a new limitation of the Hilbert spectrum on the band of frequencies encompassed in the zone limited by the following equation

$$0.90 \cdot f_0 \leq f \leq 1.10 \cdot f_0 \tag{10}$$

as illustrated in Figure 3.

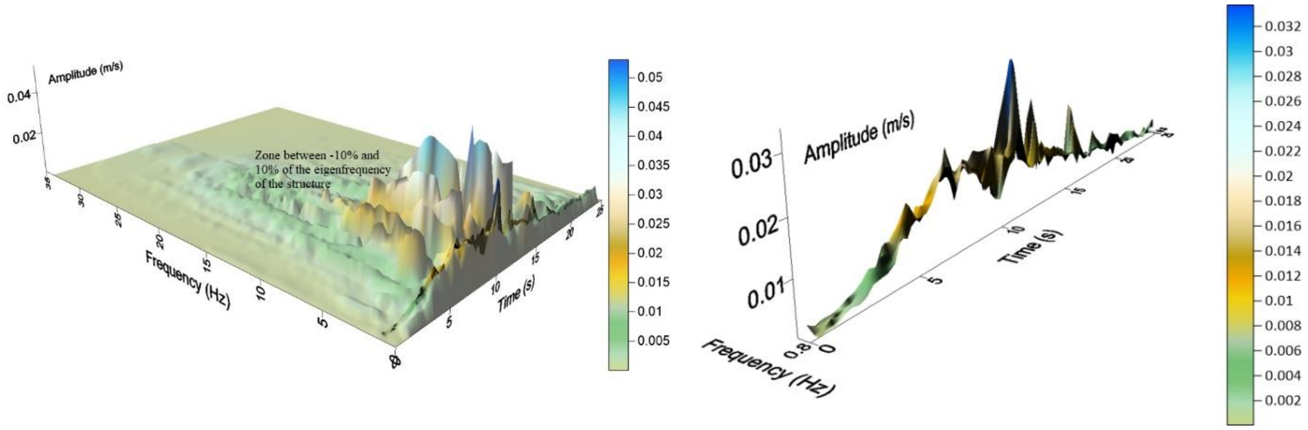

(**a**) (**b**)

Figure 3. (**a**) Limitation of the HS on the band of frequencies encompassed in the zone between 0.90 and 1.10 of the fundamental frequency f_0; (**b**) enlargement of the characteristic zone of HS.

All the above parameters were defined for the new limitation of the Hilbert spectrum and, correspondingly, were assigned as $V_{2(HHT)}$, $S_{2(HHT)}$, $A_{2(max,HHT)}$, $A_{2(mean,HHT)}$, $A_{2(dif,HHT)}$, $V_{2(Pos,HHT)}$ and $S_{2(Pos,HHT)}$, $VA_{2(max,HHT)}$, $VA_{2(mean,HHT)}$, $VA_{2(dif,HHT)}$, $A_{2(HHT)}$, and $A_{2(Pos,HHT)}$.

Additionally, the released energy from every excitation at the frequency equal to the fundamental frequency (f_0) value of a structure is presented by the calculation of the area $S_{EF(HHT)}$ of the amplitude-time section that intersects the Hilbert spectrum frequency-axis at the frequency value (f_0) (Figure 3) and defined by Equation (9).

$$S_{EF(HHT)} = \int_0^{t_{max}} a(f,t)dt \text{ where } f = f_0(\text{constant value}) \tag{11}$$

This Hilbert spectrum section's maximum and mean amplitude values were selected and designated as $A_{3(max,HHT)}$ and $A_{3(mean,HHT)}$ parameters, respectively.

The following additional seismic intensity parameters were evaluated from the combination of the above parameters, as presented in Equation (12).

$$\begin{array}{ll} S_{EF}A_{1(max)} = S_{EF} \cdot A_{1(max,HHT)} & S_{EF}A_{1(mean)} = S_{EF} \cdot A_{1(mean,HHT)} \\ S_{EF}A_{2(max)} = S_{EF} \cdot A_{2(max,HHT)} & S_{EF}A_{2(mean)} = S_{EF} \cdot A_{2(mean,HHT)} \\ S_1A_{1(mean)} = S_{1(HHT)}A_{1(mean,HHT)} & S_2A_{2(mean)} = S_{2(HHT)} \cdot A_{2(mean,HHT)} \\ S_1A_{3(max)} = S_{1(HHT)} \cdot A_{3(max,HHT)} & S_1A_{3(mean)} = S_{1(HHT)} \cdot A_{3(mean,HHT)} \end{array} \tag{12}$$

In the end, the ratio of $A_{1(mean,HHT)}$, $A_{2(mean,HHT)}$, and $A_{3(mean,HHT)}$ to $A_{1(max,HHT)}$, $A_{2(max,HHT)}$, and $A_{3(max,HHT)}$ resulted in the $A_{1(Ratio,HHT)}$, $A_{2(Ratio,HHT)}$ and $A_{3(Ratio,HHT)}$ HHT-based seismic intensity parameters respectively.

As is obvious, the computational effort for evaluating the HHT-based seismic intensity parameters is generally more extensive than the conventional ones. However, the HHT procedure provides an insight into the frequency-time history of the seismic accelerograms, which is enclosed in the HHT-based quantities.

2.3. Global Damage Index of Park and Ang

Park and Ang is a cumulative damage model [27,28] reflecting the effects of repeated cycling under seismic loading. It is the most utilized damage index ($DI_{PA,global}$) to date, mainly due to its general applicability and the precise definition of different damage states. Its most used modification is the one proposed by Kunnath et al. [29,30], and it is described by the equation

$$DI_{PA,global} = \frac{\theta_m}{\theta_u} + \frac{\beta}{M_y \theta_u} \int dE_h \tag{13}$$

where θ_m is the maximum rotation in loading history, θ_u is the ultimate rotation capacity, M_y is the yield moment, dE_h is the incremental absorbed hysteretic energy, and β is a non-negative parameter representing the effect of cyclic loading on structural damage.

A value of $DI_{PA,global}$ over 0.80 signifies total damage or complete collapse of the structure, while a value equal to zero signifies that the structure is under elastic response. According to the values of $DI_{PA,global}$, classification of the structural damage is presented in Table 1.

Table 1. Structural damage grade classification according to $DI_{PA,global}$.

Structural Damage Index	Structural Damage Degree			
	Low	Medium	Large	Total
$DI_{PA,global}$	≤ 0.3	$0.3 < DI_{PA,global} \leq 0.6$	$0.6 < DI_{PA,global} \leq 0.8$	$DI_{PA,global} > 0.80$

3. Application

A number of 100 earthquake excitations were employed for the needs of this paper. The employed excitations were applied to a seven-story reinforced concrete (RC) frame structure with a total height of 22 m, as shown in Figure 4. The structure was designed in agreement with the rules of the recent Eurocodes EC8 [31] for antiseismic structures and EC2 [32] for structural concrete. The cross-section of the beams were T-shapes with 60 cm total height, 30 cm width, and 20 cm plate thickness. The effective plate width was 1.15 m at the end bays and 1.80 m at the middle bay. The distance between frames in the three-dimensional structure was 6 m. The building was considered an "importance class II", "subsoil of type B", and "ductility class Medium". The dead weight and the seismic loading, snow, wind, and live loads were also considered. The fundamental period of the frame was equal to 0.95 s.

After applying the employed seismic acceleration time histories, nonlinear dynamic analysis of the RC frame was conducted to evaluate the structural seismic response. The hysteretic behavior of beams and columns was specified at both ends using a three-parameter Park model. Every dynamic analysis was realized using the computer software IDARC2D [33].

This model incorporates strength deterioration, stiffness degradation, slip-lock, non-symmetric response, and a trilinear monotonic envelope. The values of the above degrading parameters have been chosen from the experimental results of cyclic force-deformation characteristics of typical components of the studied structure [28,34].

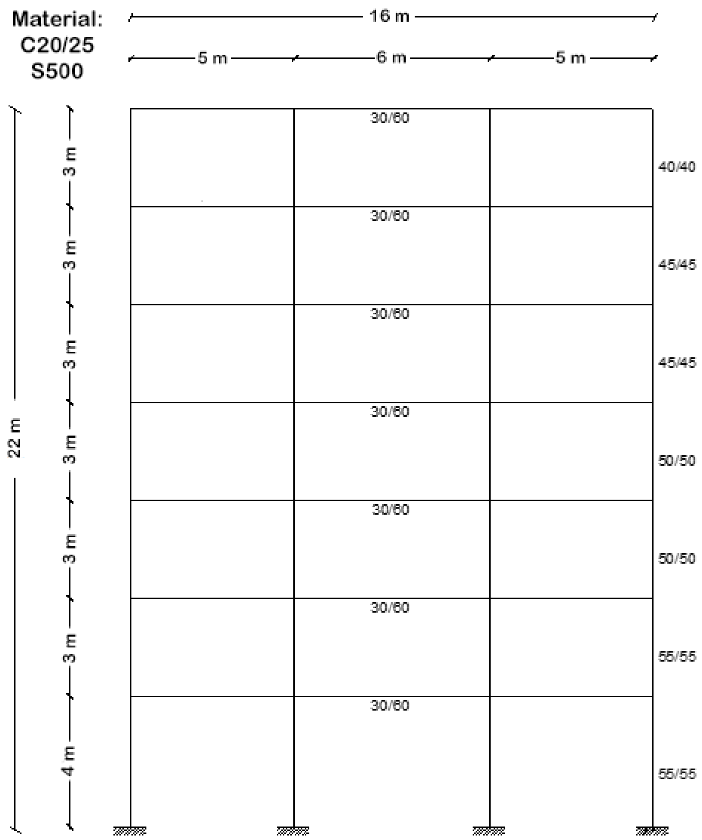

Figure 4. Reinforced concrete frame.

From the derived results of the response evaluation performing the nonlinear dynamic analysis of the structure, this article concentrates on Park and Ang's overall structural damage index ($DI_{PA,global}$). The evaluated overall structural damage indices of Park and Ang for every seismic vibration cover a broad spectrum of damage (low, medium, large, and total) for statistical reasons, as presented in Figure 5.

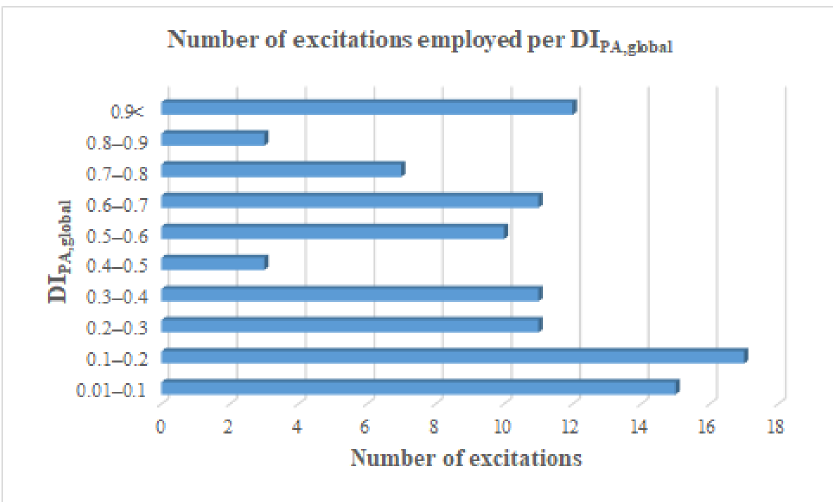

Figure 5. The number of excitations employed per $DI_{PA,global}$ range.

4. Results

4.1. Evaluation of the HHT-Based Seismic Intensity Parameters

Using the velocity time histories generated by the earthquake accelerograms, all the HHT-based seismic intensity parameters, as described above, were evaluated separately, and their elementary statistical values are presented in Table 2.

Table 2. T Statistical results of HHT-based seismic parameters.

Parameters	Statistics			
	Min Value	Max Value	Average	Standard Deviation
$S_{1(HHT)}$ (-)	153.5914	4946.3096	1350.4544	1077.2957
$V_{1(HHT)}$ (m/s)	0.2050	27.8891	5.1527	4.8203
$V_{1(Pos,HHT)}$ (m/s)	0.0597	7.4880	1.5228	1.5227
$S_{1(Pos,HHT)}$ (-)	5.8971	548.5377	86.5171	95.3434
$A_{1(max,HHT)}$ (m/s)	0.0114	0.8559	0.2363	0.1848
$A_{1(mean,HHT)}$ (m/s)	0.0005	0.1044	0.0212	0.0200
$A_{1(dif,HHT)}$ (m/s)	0.0104	0.7850	0.2151	0.1707
$A_{1(Pos,HHT)}$ (m/s)	0.0016	0.1115	0.0247	0.0196
$VA_{1(mean)}$ (m^2/s^2)	0.0002	1.1788	0.1243	0.1637
$VA_{1(max)}$ (m^2/s^2)	0.0054	7.5185	1.4392	1.6682
$VA_{1(dif,HHT)}$ (m^2/s^2)	0.0053	7.1969	1.3150	1.5428
$V_{2(HHT)}$ (m/s)	0.0000	2.1061	0.2515	0.3048
$S_{2(HHT)}$ (-)	0.0024	33.9103	12.8771	9.7173
$V_{2(Pos,HHT)}$ (m/s)	0.0000	0.5207	0.1024	0.1009
$S_{2(Pos,HHT)}$ (-)	0.0012	14.8652	4.0702	3.2751
$A_{2(max,HHT)}$ (m/s)	0.0074	0.7622	0.1567	0.1526
$A_{2(mean,HHT)}$ (m/s)	0.0006	0.2554	0.0287	0.0456
$S_{EF(HHT)}$ (-)	0.0237	10.0491	1.2100	1.4582
$A_{3(max,HHT)}$ (m/s)	0.0056	0.7422	0.1410	0.1380
$A_{3(mean,HHT)}$ (m/s)	0.0006	0.2559	0.0292	0.0460
$A_{1(Ratio,HHT)}$ (-)	0.0125	0.2241	0.0946	0.0483
$A_{2(Ratio,HHT)}$ (-)	0.0339	0.4424	0.1748	0.1040
$A_{3(Ratio,HHT)}$ (-)	0.0358	0.4957	0.1950	0.1119
$A_{1(HHT)}$ (m/s)	0.0001	0.0259	0.0055	0.0052
$A_{2(HHT)}$ (m/s)	0.0006	0.2157	0.0275	0.0407
$A_{2(Pos,HHT)}$ (m/s)	0.0009	0.1490	0.0295	0.0266
$S_{EF}A_{1(mean)}$ (m/s)	0.0000	0.3947	0.0343	0.0614
$S_{EF}A_{2(mean)}$ (m/s)	0.0000	2.5669	0.0862	0.3145
$S_{EF}A_{3(mean)}$ (m/s)	0.0000	2.5718	0.0871	0.3149
$S_{EF}A_{1(max)}$ (m/s)	0.0006	3.0521	0.3912	0.6208
$S_{EF}A_{2(max)}$ (m/s)	0.0002	7.6594	0.3452	0.8981
$S_{EF}A_{3(max)}$ (m/s)	0.0002	7.4580	0.3188	0.8620
$S_1A_{3(max)}$ (m/s)	3.2803	1193.1771	172.0672	212.8759
$S_1A_{1(mean)}$ (m/s)	0.5230	121.8580	21.4915	21.1580
$S_1A_{3(mean)}$ (m/s)	0.7957	350.8138	27.3436	43.0174
$S_2A_{2(mean)}$ (m/s)	0.0000	2.4942	0.2603	0.3402
$A_{2(dif,HHT)}$ (m/s)	0.0044	0.5721	0.1280	0.1208
$VA_{2(dif,HHT)}$ (m^2/s^2)	0.0000	1.0673	0.0538	0.1251
$VA_{2(mean)}$ (m^2/s^2)	0.0000	0.5380	0.0180	0.0660
$VA_{2(max)}$ (m^2/s^2)	0.0000	1.6053	0.0719	0.1880

4.2. Problem Formulation and ANN Framework Selection

Artificial neural networks (ANNs) refer to complex algorithms capable of imitating behaviors of biological neural systems, and they are able to learn the applied knowledge gained from experience and solve new problems in new environments. Like the structure of the human brain, they connect a number of neurons in a complex and nonlinear form. Weighted links achieve the connection between the neurons. The multi-layer feedforward perceptron (MFP) artificial neural networks have been chosen in this study. MFPs are based on a supervised learning procedure, where a number of vectors are used as input data to obtain the optimal combination of neurons' connection weights with a backpropagation algorithm for training. The ultimate target is the estimation of a set of predefined target outputs. Once the network has fit the input-output data, it forms a generalization of their relationship, and it can be used to generate output for input it was not trained on.

Artificial neural networks have been utilized in civil engineering, and many researchers have investigated their advantages in structural engineering [14–16]. In the present research, the constructed MFPs aim to model the examined parameters' ability to estimate the structures' damage potential after an earthquake. The problem in the study was approached as a function approximation problem (FA). Thus, MFP artificial neural networks were trained on a set of inputs in order to produce a set of target outputs. A large number of ANNs have evolved by trying all the potential combinations of every data set of the input HHT-based seismic parameters, and every one of them was trained with nine deferent algorithms only one time. No retraining procedure was followed for every configured ANN so that over-training models would be avoided. Over-trained models are prone to memorization, and they present extremely limited ability for generalization. In addition, all the structural damage grades (low, medium, large, and total) were considered during the ANN training. Finally, the use of the "trial and error" approach confirms the reliability of a large number of the developed MFPs, which are capable of perfectly serving the estimation of the seismic vulnerability.

The proposed procedure is an open methodology. Thus, alternative conventional and HHT-based seismic intensity parameters can be used. Additionally, alternative damage indices can be used. Finally, the proposed procedure can be applied to other structural materials and structural types (such as bridges, towers, and silos). In the latter case, appropriate damage indices must be considered.

4.3. Configuration of ANNs

The development of the MFPs requires the determination of the input and the output datasets, the choice of the optimal learning algorithm, the determination of the number of hidden layers/neurons, and the selection of the activation functions. The schematic diagram of the developed MFPs is displayed in Figure 6 and analysed below.

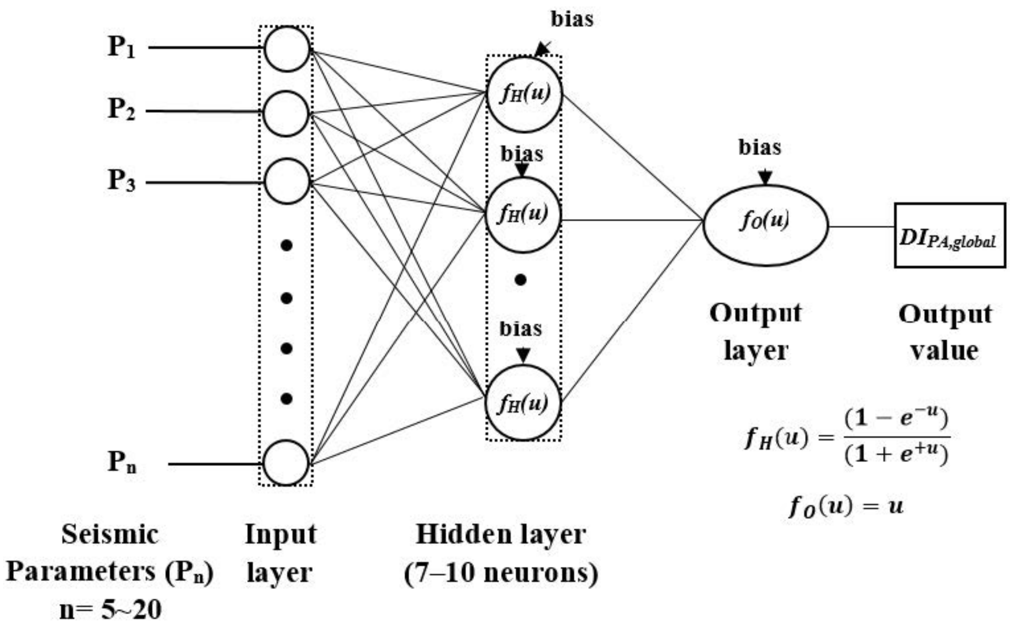

Figure 6. Schematic diagram of the developed MFPs.

The input data sets for the constructed MFP networks comprise the forty HHT-based seismic parameters, separated into two groups of twenty parameters. The division of parameters into two groups was implemented to make the calculations of ANNs with the available computational systems feasible. A separate analysis was performed following the "trial and error" approach to obtain the best network for each group. Hence, a huge number of potential input datasets that emerged by combinations of every group's parameters were tested. Each combination is comprised of at least 5 parameters. An input vector's maximum number of features was twenty as the maximum number of parameters in every group.

As target output of the formulated ANNs considered the structural damage as expressed by the overall damage index of Park and Ang ($DI_{PA,global}$). The $DI_{PA,global}$ values were derived from nonlinear dynamic analyses of the structure after applying every employed seismic accelerogram. Thus, the output layer of the MFPs consisted of one neuron presenting the value of $DI_{PA,global}$.

All the evolved MFP networks had one hidden layer to keep their architecture as simple as possible. This choice was based on the ability of feedforward perceptron networks with one hidden layer to precisely approach functions f(x): Rn→R1, as well as on their already proven efficiency by numerous relevant investigations [12,13]. The number of neurons in the hidden layer was also investigated. ANN models with 7 to 10 hidden neurons were tested. This range was chosen based on the number of available excitations (100) in the source data as training vectors. As a result, four additional networks were calculated for every produced ANN by combining the examined seismic parameters of every group.

At last, as presented in Table 3, nine different training backpropagation algorithms were utilized in the formulation of the multilinear feedforward networks. Moreover, a sigmoid, precisely the tangent hyperbolic (TanH) transfer function f_H, was employed for the hidden layer, while the choice of linear activation function was made for the output layer.

Table 3. Backpropagation training algorithms of the developed ANNs.

Backpropagation (BP) Training Algorithms	
Levenberg–Marquardt (LM)	Powell–Beale conjugate gradient (CGB)
BFGS quasi-Newton (BFG)	Fletcher–Powell conjugate gradient (CGF)
Resilient backpropagation (RP)	Polak–Ribiere conjugate gradient (CGP)
Scaled conjugate gradient (BP)	One step secant (OSS)
Gradient descent with momentum and adaptive linear (GDX)	

4.4. Calculation of ANNs

The MATLAB 2019a [35] software program was used to develop and evaluate the formulated artificial networks according to the flowchart in Figure 7. Due to the extensive number of developed networks with training algorithms that are not always GPU capable, a parallelized environment of ten virtual instances of the program MATLAB was utilized.

Additionally, each instance was equipped with two MATLAB workers and had access to 12 GB of memory and **8** i9-9900k threads.

An appropriate MATLAB script was developed so all the ANNs could be formulated and trained with the employed training algorithms with the best use of the available resources. The performance evaluation parameters R correlation coefficient and the mean squared error (MSE) were adopted and calculated to compare the MFP networks. From the total employed seismic excitations, a 70% was used as the training set, 15% was used as the testing set, and 15% was used as the validation set.

In statistics, the R coefficient between two variables reflects the strength and the direction of a linear relationship and takes values between −1 (total negative linear correlation and +1 (total positive linear correlation). The MSE is an average of the absolute difference between the target values, calculated by nonlinear dynamic analysis values of $DI_{PA,global}$, and the corresponding ones evaluated by the constructed ANNs.

The basic statistics of R and MSE values and their classification for the constructed ANNs are presented in the following Tables. Specifically, Tables 4–7 present the minimum (min), maximum (max), mean, and standard deviation (st.dev.) of the evaluated R and MSE values. The values are presented for every training algorithm and every investigated number of neurons in the hidden layer for both groups of input data. In addition, Tables 8–11 present the classification of MFPs according to an R absolute value equal to or greater than 0.90 and their classification according to MSE values. As displayed in Tables 8–11, the calculated MFPs for both coefficients (R, MSE) are categorized into three classes.

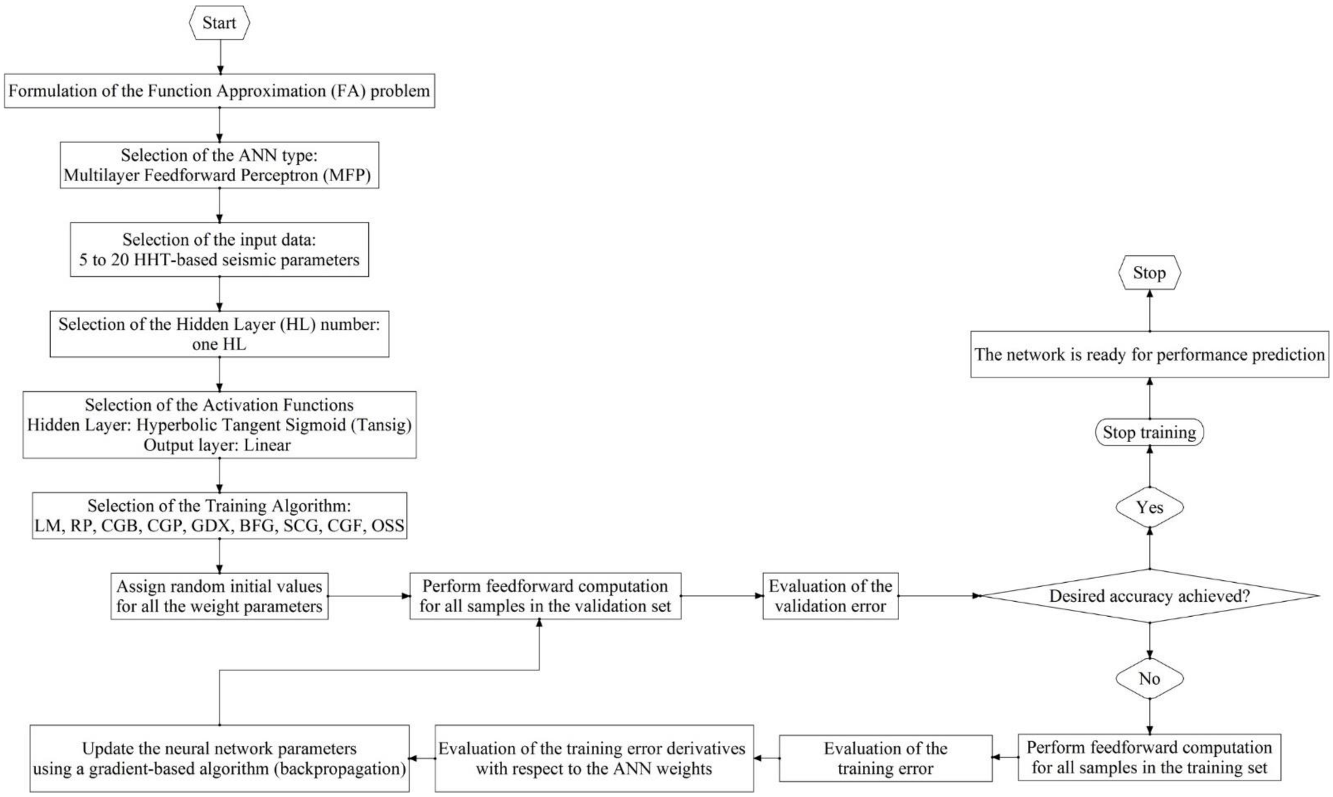

Figure 7. Flowchart of ANN computational procedures.

Table 4. Statistics of R—ANNs with input parameters of Group 1.

Group 1—R Statistics								
Training Algorithm	**7-Neuron Hidden Layer**				**8-Neuron Hidden Layer**			
	Min	**Max**	**Mean**	**st.dev.**	**Min**	**Max**	**Mean**	**st.dev.**
trainlm	−0.6317	0.9841	0.9042	0.0514	−0.5746	0.9882	0.9028	0.0528
trainbfg	−0.7944	0.9642	0.8435	0.1083	−0.7071	0.9616	0.8459	0.1013
trainrp	−0.7916	0.9601	0.8173	0.1193	−0.7038	0.9610	0.8182	0.1168
trainscg	−0.8194	0.9618	0.8376	0.1149	−0.5916	0.9610	0.8391	0.1075
traincgb	−0.6282	0.9700	0.8524	0.1051	−0.6858	0.9633	0.8530	0.1004
traincgf	−0.7216	0.9626	0.8393	0.1123	−0.5956	0.9616	0.8432	0.1048
traincgp	−0.6849	0.9681	0.8410	0.1111	−0.6858	0.9618	0.8416	0.1060
trainoss	−0.6953	0.9551	0.8346	0.1127	−0.6866	0.9587	0.8366	0.1052
traingdx	−0.8512	0.9529	0.5966	0.3801	−0.8566	0.9490	0.5958	0.3822
	9-Neuron Hidden Layer				10-Neuron Hidden Layer			
	min	max	mean	st.dev.	min	max	mean	st.dev.
trainlm	−0.6315	0.9861	0.9017	0.0537	−0.5106	0.9838	0.9008	0.0548
trainbfg	−0.6329	0.9622	0.8479	0.0956	−0.6748	0.9674	0.8495	0.0918
trainrp	−0.6880	0.9571	0.8191	0.1150	−0.7202	0.9622	0.8191	0.1147
trainscg	−0.7171	0.9721	0.8398	0.1032	−0.6387	0.9656	0.8403	0.1005
traincgb	−0.6102	0.9661	0.8536	0.0963	−0.6650	0.9692	0.8538	0.0937
traincgf	−0.7120	0.9618	0.8455	0.1000	−0.6384	0.9627	0.8470	0.0963
traincgp	−0.6248	0.9616	0.8420	0.1017	−0.6650	0.9658	0.8423	0.0990
trainoss	−0.7067	0.9607	0.8379	0.0994	−0.6939	0.9584	0.8386	0.0959
traingdx	−0.8554	0.9524	0.5910	0.3853	−0.8609	0.9512	0.5829	0.3904

Table 5. Statistics of MSE—ANNs with input parameters of Group 1.

Group 1—MSE Statistics								
Training Algorithm	**7-Neuron Hidden Layer**				**8-Neuron Hidden Layer**			
	Min	**Max**	**Mean**	**st.dev.**	**Min**	**Max**	**Mean**	**st.dev.**
trainlm	0.0029	0.3214	0.0183	0.0103	0.0023	0.3745	0.0187	0.0107
trainbfg	0.0066	0.4275	0.0266	0.0154	0.0070	0.4322	0.0264	0.0149
trainrp	0.0072	0.5305	0.0309	0.0180	0.0071	0.5626	0.0309	0.0182
trainscg	0.0069	0.5355	0.0272	0.0156	0.0070	0.4774	0.0271	0.0151
traincgb	0.0054	0.3952	0.0249	0.0146	0.0067	0.4553	0.0249	0.0143
traincgf	0.0067	0.5486	0.0270	0.0155	0.0070	0.5340	0.0265	0.0149
traincgp	0.0058	0.4636	0.0267	0.0153	0.0070	0.4553	0.0267	0.0150
trainoss	0.0081	0.4828	0.0280	0.0158	0.0074	0.4388	0.0279	0.0153
traingdx	0.0084	0.7099	0.0595	0.0534	0.0091	1.0021	0.0618	0.0579
	9-Neuron Hidden Layer				10-Neuron Hidden Layer			
	min	max	mean	st.dev.	min	max	mean	st.dev.
trainlm	0.0026	0.4003	0.0190	0.0110	0.0030	0.4343	0.0192	0.0114
trainbfg	0.0069	0.4309	0.0262	0.0145	0.0059	0.4576	0.0260	0.0141
trainrp	0.0077	0.9272	0.0309	0.0183	0.0069	0.6747	0.0310	0.0187
trainscg	0.0050	0.6328	0.0271	0.0148	0.0062	0.7438	0.0271	0.0148
traincgb	0.0062	0.4318	0.0249	0.0141	0.0056	0.6200	0.0249	0.0140
traincgf	0.0069	0.4737	0.0262	0.0146	0.0068	0.5245	0.0260	0.0144
traincgp	0.0069	0.4597	0.0267	0.0147	0.0062	0.6200	0.0268	0.0147
trainoss	0.0071	0.5018	0.0278	0.0149	0.0075	0.6408	0.0277	0.0147
traingdx	0.0086	0.9054	0.0648	0.0626	0.0087	0.9933	0.0685	0.0677

Table 6. Statistics of R—ANNs with input parameters of Group 2.

Group 2—R Statistics								
Training Algorithm	**7-Neuron Hidden Layer**				**8-Neuron Hidden Layer**			
	Min	**Max**	**Mean**	**st.dev.**	**Min**	**Max**	**Mean**	**st.dev.**
trainlm	−0.7834	0.9730	0.8824	0.0494	−0.8028	0.9706	0.8818	0.0502
trainbfg	−0.7816	0.9357	0.8439	0.0594	−0.7483	0.9396	0.8443	0.0590
trainrp	−0.7842	0.9248	0.8305	0.0692	−0.7366	0.9312	0.8298	0.0709
trainscg	−0.7808	0.9317	0.8399	0.0655	−0.7462	0.9397	0.8394	0.0657
traincgb	−0.7319	0.9450	0.8475	0.0604	−0.8165	0.9441	0.8474	0.0607
traincgf	−0.7618	0.9350	0.8431	0.0640	−0.7744	0.9364	0.8433	0.0640
traincgp	−0.7618	0.9350	0.8420	0.0629	−0.7661	0.9327	0.8415	0.0636
trainoss	−0.7750	0.9289	0.8397	0.0607	−0.8062	0.9312	0.8396	0.0598
traingdx	−0.8783	0.9161	0.6750	0.3145	−0.8764	0.9184	0.6622	0.3236
	9-Neuron Hidden Layer				10-Neuron Hidden Layer			
	min	max	mean	st.dev.	min	max	mean	st.dev.
trainlm	−0.7400	0.9698	0.8812	0.0513	−0.7718	0.9668	0.8807	0.0519
trainbfg	−0.8010	0.9400	0.8444	0.0595	−0.6828	0.9406	0.8445	0.0595
trainrp	−0.7421	0.9271	0.8286	0.0735	−0.7388	0.9299	0.8275	0.0756
trainscg	−0.7310	0.9326	0.8387	0.0662	−0.7900	0.9337	0.8377	0.0680
traincgb	−0.7702	0.9417	0.8469	0.0618	−0.7683	0.9428	0.8463	0.0626
traincgf	−0.8038	0.9417	0.8429	0.0655	−0.7986	0.9383	0.8426	0.0663
traincgp	−0.7792	0.9351	0.8409	0.0640	−0.7785	0.9394	0.8403	0.0649
trainoss	−0.7717	0.9373	0.8391	0.0601	−0.7550	0.9388	0.8385	0.0602
traingdx	−0.8769	0.9152	0.6483	0.3341	−0.8766	0.9224	0.6326	0.3464

Table 7. T Statistics of MSE—ANNs with input parameters of Group 2.

Group 2—MSE Statistics								
Training Algorithm	**7-Neuron Hidden Layer**				**8-Neuron Hidden Layer**			
	Min	**Max**	**Mean**	**st.dev.**	**Min**	**Max**	**Mean**	**st.dev.**
trainlm	0.0049	0.3890	0.0225	0.0113	0.0055	0.6813	0.0228	0.0119
trainbfg	0.0115	0.6292	0.0272	0.0097	0.0108	0.6749	0.0273	0.0100
trainrp	0.0134	0.4977	0.0298	0.0117	0.0122	0.4258	0.0300	0.0122
trainscg	0.0122	0.3255	0.0276	0.0100	0.0109	0.6220	0.0278	0.0104
traincgb	0.0099	0.3728	0.0263	0.0093	0.0100	0.4400	0.0264	0.0096
traincgf	0.0116	0.3831	0.0270	0.0098	0.0113	0.4416	0.0270	0.0100
traincgp	0.0119	0.3452	0.0272	0.0096	0.0119	0.4335	0.0274	0.0099
trainoss	0.0126	0.5109	0.0280	0.0099	0.0122	0.7328	0.0281	0.0100
traingdx	0.0149	1.0202	0.0500	0.0407	0.0144	1.3593	0.0529	0.0446
	9-Neuron Hidden Layer				10-Neuron Hidden Layer			
	min	max	mean	st.dev.	min	max	mean	st.dev.
trainlm	0.0055	0.4265	0.0230	0.0124	0.0060	0.5154	0.0233	0.0129
trainbfg	0.0107	0.4202	0.0273	0.0102	0.0106	6.7141	0.0274	0.0124
trainrp	0.0129	0.4869	0.0303	0.0129	0.0124	0.3849	0.0306	0.0135
trainscg	0.0119	0.3476	0.0280	0.0107	0.0119	0.4225	0.0282	0.0113
traincgb	0.0105	0.6390	0.0265	0.0100	0.0102	0.6842	0.0267	0.0104
traincgf	0.0105	0.4828	0.0272	0.0105	0.0110	0.7971	0.0273	0.0109
traincgp	0.0115	0.3930	0.0275	0.0103	0.0108	0.4685	0.0277	0.0107
trainoss	0.0111	0.3888	0.0283	0.0103	0.0112	0.6655	0.0285	0.0107
traingdx	0.0150	1.1226	0.0563	0.0494	0.0139	1.0971	0.0600	0.0541

Table 8. Classification of R—ANNs with input parameters of Group 1.

Group 1_ Classification of R										
7 Neurons in the Hidden Layer		**Training Function of ANNs**								
		Train-lm	**Train-bfg**	**Train-rp**	**Train-scg**	**Train-cgb**	**Train-cgf**	**Train-cgp**	**Train-oss**	**Train-gdx**
$R \geq 0.95$	(%) of ANNs	3.824	0.025	0.003	0.012	0.065	0.027	0.026	0.003	0.000
$0.92 \leq R < 0.95$	(%) of ANNs	39.795	5.825	1.796	4.789	8.921	6.053	5.833	2.933	2.433
$0.90 \leq R < 0.92$	(%) of ANNs	25.681	18.798	9.619	17.356	22.611	18.198	18.511	14.854	11.814
	Total (%)	69.300	24.623	11.415	22.145	31.532	24.251	24.344	17.787	14.247
8 Neurons in the Hidden Layer		Training function of ANNs								
		train-lm	train-bfg	train-rp	train-scg	train-cgb	train-cgf	train-cgp	train-oss	train-gdx
$R \geq 0.95$	(%) of ANNs	3.567	0.026	0.004	0.013	0.054	0.025	0.021	0.003	0.000
$0.92 \leq R < 0.95$	(%) of ANNs	38.888	6.099	2.105	4.828	8.836	6.400	5.744	3.062	2.542
$0.90 \leq R < 0.92$	(%) of ANNs	25.782	18.693	9.964	16.728	21.995	18.488	17.843	14.663	11.897
	Total (%)	68.237	24.792	12.069	21.556	30.831	24.888	23.587	17.725	14.439
9 Neurons in the Hidden Layer		Training function of ANNs								
		train-lm	train-bfg	train-rp	train-scg	train-cgb	train-cgf	train-cgp	train-oss	train-gdx
$R \geq 0.95$	(%) of ANNs	3.429	0.028	0.007	0.014	0.051	0.028	0.025	0.003	0.000
$0.92 \leq R < 0.95$	(%) of ANNs	38.294	6.350	2.445	4.895	8.871	6.681	5.622	3.176	2.639
$0.90 \leq R < 0.92$	(%) of ANNs	25.803	18.640	10.333	16.402	21.433	18.632	17.407	14.492	11.871
	Total (%)	67.526	24.990	12.778	21.297	30.304	25.313	23.029	17.668	14.510
10 Neurons in the Hidden Layer		Training function of ANNs								
		train-lm	train-bfg	train-rp	train-scg	train-cgb	train-cgf	train-cgp	train-oss	train-gdx
$R \geq 0.95$	(%) of ANNs	3.400	0.029	0.009	0.015	0.053	0.030	0.023	0.004	0.000
$0.92 \leq R < 0.95$	(%) of ANNs	37.896	6.681	2.720	4.964	8.863	6.982	5.654	3.301	2.672
$0.90 \leq R < 0.92$	(%) of ANNs	25.542	18.710	10.626	16.184	21.061	18.586	16.933	14.224	11.744
	Total (%)	66.838	25.391	13.346	21.148	29.924	25.568	22.587	17.525	14.416

Table 9. Classification of MSE—ANNs with input parameters of Group 1.

Group 1_ Classification of MSE										
7 Neurons in the Hidden Layer		**Training Function of ANNs**								
		Train-lm	**Train-bfg**	**Train-rp**	**Train-scg**	**Train-cgb**	**Train-cgf**	**Train-cgp**	**Train-oss**	**Train-gdx**
MSE ≤ 0.02	(%) of ANNs	73.845	39.738	22.742	37.373	47.960	39.114	39.759	32.559	24.172
0.02 < MSE ≤ 0.05	(%) of ANNs	24.297	53.256	67.244	55.197	46.043	53.267	53.122	59.590	35.775
MSE > 0.05	(%) of ANNs	1.858	7.006	10.013	7.430	5.997	7.619	7.120	7.851	40.053
8 Neurons in the Hidden Layer		Training function of ANNs								
		train-lm	train-bfg	train-rp	train-scg	train-cgb	train-cgf	train-cgp	train-oss	train-gdx
MSE ≤ 0.02	(%) of ANNs	72.489	39.623	23.289	36.359	46.871	39.802	38.576	32.031	24.230
0.02 < MSE ≤ 0.05	(%) of ANNs	25.411	53.858	66.622	56.650	47.445	53.435	54.580	60.565	35.736
MSE > 0.05	(%) of ANNs	2.100	6.519	10.089	6.991	5.684	6.763	6.844	7.404	40.033
9 Neurons in the Hidden Layer		Training function of ANNs								
		train-lm	train-bfg	train-rp	train-scg	train-cgb	train-cgf	train-cgp	train-oss	train-gdx
MSE ≤ 0.02	(%) of ANNs	71.505	39.575	23.939	35.687	46.013	40.113	37.558	31.539	24.049
0.02 < MSE ≤ 0.05	(%) of ANNs	26.190	54.330	65.894	57.610	48.541	53.649	55.862	61.414	35.374
MSE > 0.05	(%) of ANNs	2.305	6.094	10.167	6.703	5.446	6.238	6.580	7.048	40.578
10 Neurons in the Hidden Layer		Training function of ANNs								
		train-lm	train-bfg	train-rp	train-scg	train-cgb	train-cgf	train-cgp	train-oss	train-gdx
MSE ≤ 0.02	(%) of ANNs	70.517	39.710	24.408	35.199	45.344	40.257	36.821	31.122	23.675
0.02 < MSE ≤ 0.05	(%) of ANNs	26.923	54.526	65.203	58.330	49.395	53.846	56.803	62.073	34.845
MSE > 0.05	(%) of ANNs	2.560	5.765	10.389	6.471	5.261	5.897	6.376	6.805	41.480

Table 10. Classification of R—ANNs with input parameters of Group 2.

Group 2_ Classification of R										
7 Neurons in the Hidden Layer		**Training Function of ANNs**								
		Train-lm	**Train-bfg**	**Train-rp**	**Train-scg**	**Train-cgb**	**Train-cgf**	**Train-cgp**	**Train-oss**	**Train-gdx**
R ≥ 0.95	(%) of ANNs	0.024	0.000	0.000	0.000	0.000	0.000	0.000	0.000	0.000
0.92 ≤ R < 0.95	(%) of ANNs	11.006	0.061	0.001	0.011	0.102	0.046	0.023	0.003	0.000
0.90 ≤ R < 0.92	(%) of ANNs	26.009	1.431	0.627	0.839	2.351	1.709	1.094	0.527	0.204
	Total (%)	37.039	1.492	0.628	0.850	2.453	1.755	1.117	0.530	0.204
8 Neurons in the Hidden Layer		Training function of ANNs								
		train-lm	train-bfg	train-rp	train-scg	train-cgb	train-cgf	train-cgp	train-oss	train-gdx
R ≥ 0.95	(%) of ANNs	0.031	0.000	0.000	0.000	0.000	0.000	0.000	0.000	0.000
0.92 ≤ R< 0.95	(%) of ANNs	10.794	0.067	0.004	0.012	0.113	0.057	0.025	0.004	0.000
0.90 ≤ R < 0.92	(%) of ANNs	25.706	1.687	0.874	1.021	2.586	2.031	1.250	0.616	0.268
	Total (%)	36.531	1.754	0.878	1.033	2.699	2.088	1.275	0.620	0.268
9 Neurons in the Hidden Layer		Training function of ANNs								
		train-lm	train-bfg	train-rp	train-scg	train-cgb	train-cgf	train-cgp	train-oss	train-gdx
R ≥ 0.95	(%) of ANNs	0.030	0.000	0.000	0.000	0.000	0.000	0.000	0.000	0.000
0.92 ≤ R< 0.95	(%) of ANNs	10.717	0.073	0.006	0.014	0.123	0.067	0.029	0.004	0.000
0.90 ≤ R < 0.92	(%) of ANNs	25.692	1.943	1.107	1.155	2.871	2.373	1.415	0.737	0.328
	Total (%)	36.439	2.016	1.113	1.169	2.994	2.440	1.444	0.741	0.328
10 Neurons in the Hidden Layer		Training function of ANNs								
		train-lm	train-bfg	train-rp	train-scg	train-cgb	train-cgf	train-cgp	train-oss	train-gdx
R ≥ 0.95	(%) of ANNs	0.032	0.000	0.000	0.000	0.000	0.000	0.000	0.000	0.000
0.92 ≤ R< 0.95	(%) of ANNs	10.723	0.086	0.007	0.017	0.141	0.080	0.031	0.006	0.000
0.90 ≤ R < 0.92	(%) of ANNs	25.727	2.238	1.367	1.325	3.160	2.643	1.577	0.849	0.377
	Total (%)	36.482	2.324	1.374	1.342	3.301	2.723	1.608	0.855	0.377

Table 11. Classification of MSE—ANNs with input parameters of Group 2.

Group 2_ Classification of MSE										
7 Neurons in the Hidden Layer		**Training Function of ANNs**								
		Train-lm	**Train-bfg**	**Train-rp**	**Train-scg**	**Train-cgb**	**Train-cgf**	**Train-cgp**	**Train-oss**	**Train-gdx**
MSE ≤ 0.02	(%) of ANNs	50.924	9.995	6.220	8.388	13.713	11.564	9.326	6.209	3.938
0.02 < MSE ≤ 0.05	(%) of ANNs	46.544	86.798	88.399	88.132	83.578	85.282	87.567	90.324	63.407
MSE > 0.05	(%) of ANNs	2.533	3.207	5.381	3.480	2.709	3.153	3.107	3.467	32.655
8 Neurons in the Hidden Layer		Training function of ANNs								
		train-lm	train-bfg	train-rp	train-scg	train-cgb	train-cgf	train-cgp	train-oss	train-gdx
MSE ≤ 0.02	(%) of ANNs	50.028	10.902	7.247	8.975	14.576	12.550	9.914	6.722	4.214
0.02 < MSE ≤ 0.05	(%) of ANNs	47.193	85.896	86.977	87.449	82.668	84.300	86.904	89.805	60.522
MSE > 0.05	(%) of ANNs	2.778	3.202	5.776	3.575	2.757	3.150	3.182	3.473	35.264
9 Neurons in the Hidden Layer		Training function of ANNs								
		train-lm	train-bfg	train-rp	train-scg	train-cgb	train-cgf	train-cgp	train-oss	train-gdx
MSE ≤ 0.02	(%) of ANNs	49.432	11.812	8.166	9.455	15.237	13.451	10.431	7.158	4.412
0.02 < MSE ≤ 0.05	(%) of ANNs	47.556	84.887	85.491	86.791	81.856	83.177	86.251	89.213	57.669
MSE > 0.05	(%) of ANNs	3.012	3.301	6.344	3.754	2.907	3.372	3.318	3.628	37.919
10 Neurons in the Hidden Layer		Training function of ANNs								
		train-lm	train-bfg	train-rp	train-scg	train-cgb	train-cgf	train-cgp	train-oss	train-gdx
MSE ≤ 0.02	(%) of ANNs	48.984	12.710	8.854	9.912	15.907	14.177	10.927	7.529	4.492
0.02 < MSE ≤ 0.05	(%) of ANNs	47.765	83.859	84.351	86.051	80.954	82.254	85.507	88.662	54.944
MSE > 0.05	(%) of ANNs	3.251	3.431	6.795	4.037	3.139	3.568	3.567	3.809	40.564

5. Discussion

The investigation of the results reveals that all the training algorithms present a number of configured ANNs whose performance in the estimation of the structural damage through the examined parameters is described with a very high R correlation coefficient (R > 0.95) and very small MSE (MSE < 0.02). However, observing Tables 4–7, it becomes obvious that the most efficient training algorithm is the Levenberg–Marquardt (LM) algorithm for the first group of input data preventing the most significant configured MFP networks with mean correlation coefficient ranging from 0.9008 to 0.9042 and with mean MSE ranging from 0.0183 to 0.0192. Additionally, the best MFP model was trained by the LM algorithm for input datasets of the first group of parameters with an absolute maximum value of R equal to 0.9882 and a minimum MSE value equal to 0.0023 for 8 neurons in the hidden layer.

Furthermore, depending on the number of neurons in the hidden layer, ANN cases trained with the LM algorithm present R > 0.90 with a percentage up to 66.30% for the first group of parameters and up to 37.04% for the second group of parameters. Likewise, most ANN cases trained with the same algorithm are able to predict the $DI_{PA,global}$ damage index with MSE less than 0. Similarly, depending on the number of neurons in the hidden layer, up to 73.85% for the group 1 parameters and up to 50.92% for the group 2 can predict the $\mathrm{DI}_{\mathrm{PA,global}}$ damage index with MSE less than 0.02. This means that at least 66.30% of the first group and 37.04% for the second group of parameters are able to develop ANNs with excellent predictive accuracy (with R > 0.90 και MSE < 0.02 simultaneously).

Concluding, the very high correlation coefficient R combined with a very small mean squared error (MSE) are effective quality indicators of the results. This fact confirms that the proposed methodology provides satisfactory results in predicting the utilized damage index and is an efficient tool using artificial intelligence procedures.

One possible application of the proposed methodology is to use the trained ANN to predict the damage indicator of a building for the early identification of its structural damage immediately after a seismic event, under the condition that all the required seismic intensity parameters have been evaluated instantly after the event by processing regional seismic record data.

6. Conclusions

This research designates the performance of forty HHT-based seismic intensity parameters, calculated for an RC-framed structure, to predict seismic damage through artificial neural network models. A number of 75,051,360 MFPs were developed, and their investigation revealed the increased ability of the examined parameters to predict the structural damage proving their interrelation with the overall structural damage index of Park and Ang. For this reason, the structure of the MFP artificial network with one hidden layer was chosen. The calculation of the configured MFPs led to the development of high-performance mathematical models which are able to express the probability that a structure will experience a damage situation, as expressed by $DI_{PA,global}$, with high accuracy.

For the calculation of the MFPs, nine training algorithms were utilized, which led to a significant percentage of ANNs with a very high coefficient correlation ($R > 0.90$) and low MSE ($MSE < 0.02$). The most efficient of them turned out to be the LM algorithm. A number of 8.339.040 ANNs were configured with the LM algorithm from two groups of twenty parameters. These seismic parameters created MFP networks of a high explanation of variance of $DI_{PA,global}$ (with $R > 0.90$) and a very low MSE ($MSE < 0.02$), simultaneously with a percentage up to 66.30% for the first group and up to 37.04% for the second group of parameters. According to the classification table of the $DI_{PA,global}$, an MSE coefficient with values lower than 0.02 cannot essentially change the class of structural damage caused by a seismic excitation.

The numerical results reveal that the 40 examined HHT-based seismic intensity parameters provided adequate results, evaluating the used damage index with sufficient accuracy, justified by many seismic excitations with very high correlation coefficient R and a very small mean squared error. Thus, the proposed methodology is a valuable complement to existing artificial intelligence procedures.

Additionally, it is observed that the best performance of all the investigated statistical coefficients was displayed among the ANNs with nine neurons in the hidden layer, which used the LM algorithm. In particular, the MFPs with nine neurons in the hidden layer for the input datasets of Group 1 accomplished an estimation of damage with an R correlation coefficient value upon the value of 0.9883 and a value of MSE that can be reduced until the values of 0.0023.

The conditions that must be considered for applying the proposed procedure are first that the number of the used seismic intensity parameters and accelerograms is sufficiently large for the appropriate training of the ANN. In addition, the numerical values of the utilized damage index must be considered to cover all the structural damage grades (low, medium, large, and total) during the ANN training.

It is obvious that all the above outcomes confirm the capability of the examined seismic intensity parameters to predict the induced seismic damage to the RC-framed structures. In addition, the investigated HHT-based seismic parameters are presented as effective descriptors of the seismic damage potential and, thus, are able to stand as helpful tools for a performance-based design of framed structures. Consequently, the developed ANN models using HHT-based seismic parameters can be considered an essential method for the early identification of structural vulnerability.

Author Contributions: Conceptualization, M.T. and A.E.; methodology, M.T., A.E., I.A. and L.V.; software, M.T., A.E., I.A. and L.V.; validation, I.A. and L.V.; formal analysis, M.T., A.E., I.A. and L.V.; investigation, M.T., A.E., I.A. and L.V.; resources, M.T., A.E., I.A. and L.V.; data curation, M.T., A.E., I.A. and L.V.; writing—original draft preparation, M.T. and A.E.; writing—review and editing, A.E.; visualization, M.T., A.E., I.A. and L.V.; supervision, A.E.; project administration, A.E.; funding acquisition, N/A. All authors have read and agreed to the published version of the manuscript.

Funding: This research received no external funding.

Institutional Review Board Statement: The study did not require ethical approval.

Informed Consent Statement: Not applicable.

Data Availability Statement: The study did not report any data.

Conflicts of Interest: The authors declare no conflict of interest.

References

1. Elenas, A. Correlation between seismic acceleration parameters and overall structural damage indices of buildings. *Soil Dyn. Earthq. Eng.* **2000**, *20*, 93–100. [CrossRef]
2. Elenas, A.; Meskouris, K. Correlation study between seismic acceleration parameters and damage indices of structures. *Eng. Struct.* **2001**, *23*, 698–704. [CrossRef]
3. Alvanitopoulos, P.F.; Andreadis, I.; Elenas, A. A genetic algorithm for the classification of earthquake damages in buildings. In Proceedings of the 5th IFIP Conference on Artificial Intelligence Applications & Innovations, Thessaloniki, Greece, 23–25 April 2009; pp. 341–346.
4. Alvanitopoulos, P.F.; Andreadis, I.; Elenas, A. A New Algorithm for the Classification of Earthquake Damages in Structures. In Proceedings of the 5th IASTED Conference on Signal Processing, Pattern Recognition and Applications, Innsbruck, Austria, 13–15 February 2008; pp. 151–156.
5. Alvanitopoulos, P.F.; Andreadis, I.; Elenas, A. Neuro-fuzzy techniques for the classification of earthquake damages in buildings. *Measurement* **2010**, *43*, 797–809. [CrossRef]
6. Elenas, A. Seismic-Parameter-Based Statistical Procedure for the Approximate Assessment of Structural Damage. *Math. Probl. Eng.* **2014**, *2014*, 916820. [CrossRef]
7. Elenas, A. Interdependency between seismic acceleration parameters and the behavior of structures. *Soil Dyn. Earthq. Eng.* **1997**, *16*, 317–322. [CrossRef]
8. Nanos, N.; Elenas, A.; Ponterosso, P. Correlation of different strong motion duration parameters and damage indicators of reinforced concrete structures. In Proceedings of the 14th World Conference on Earthquake Engineering, Beijing, China, 12–17 October 2008.
9. Kostinakis, K.; Athanatopoulou, A.; Morfidis, K. Correlation between ground motion intensity measures and seismic damage of 3D R/C buildings. *Eng. Struct.* **2015**, *82*, 151–167. [CrossRef]
10. Tyrtaiou, M.; Elenas, A. Seismic Damage Potential Described by Intensity Parameters Based on Hilbert-Huang Transform Analysis and Fundamental Frequency of Structures. *Earthq. Struct.* **2020**, *18*, 507–517.
11. Tyrtaiou, M.; Elenas, A. Novel Hilbert spectrum-based seismic intensity parameters interrelated with structural damage. *Earthq. Struct.* **2019**, *16*, 197–208.
12. Lautour, O.R.; Omenzetter, P. Prediction of seismic-induced structural damage using artificial neural networks. *Eng. Struct.* **2009**, *31*, 600–606. [CrossRef]
13. Morfidis, K.; Kostinakis, K. Approaches to the rapid seismic damage prediction of r/c buildings using artificial neural networks. *Eng. Struct.* **2018**, *165*, 120–141. [CrossRef]
14. Tsou, P.; Shen, M.H. Structural Damage Detection and Identification Using Neural Network. In Proceedings of the 34thA-IAA/ASME/ASCEAHS/ASC, Structural, Structural Dynamics and Materials Conference, AIAA/ASME Adaptive Structural Forum, La Jolla, CA, USA, 19–22 April 1993.
15. Wu, X.; Ghaboussi, J.; Garrett, J. Use of Neural Network in Detection of Structural Damage. *Comput. Struct.* **1992**, *42*, 649–659. [CrossRef]
16. Zhao, J.; Ivan, J.N.; DeWold, J.T. Structural Damage Detection Using Artificial Neural Networks. *J. Infrastructural Syst.* **1998**, *13*, 182–189. [CrossRef]
17. Zameeruddin, M.; Sangle, K.K. Damage assessment of reinforced concrete moment resisting frames using performance-based seismic evaluation procedure. *J. King Saud Univ. Eng. Sci.* **2021**, *33*, 227–239. [CrossRef]
18. Zameeruddin, M.; Sangle, K.K. Review on Recent developments in the performance-based seismic design of reinforced concrete structures. *Structures* **2016**, *6*, 119–133. [CrossRef]
19. Loh, C.H.; Chao, S.H. The Use of Damage Function in Performanced-Based Seismic Design of Structures. In Proceedings of the 13th World Conference on Earthquake Engineering, Vancouver, BC, Canada, 1–6 August 2004.
20. Gholizadeh, S.; Fattahi, F. Damage-controlled performance-based design optimization of steel moment frames. *Struct. Des. Tall Spec. Build.* **2018**, *27*, e1498. [CrossRef]
21. Jiang, H.J.; Chen, L.Z.; Chen, Q. Seismic Damage Assessment and Performance Levels of Reinforced Concrete Members. In Proceedings of the 12th East Asia-Pacific Conference on Structural Engineering and Construction, Hong Kong, China, 26–28 January 2011.
22. Huang, N.; Shen, Z.; Long, S.R.; Wu, M.C.; Shih, H.H.; Zheng, Q.; Yen, N.; Tung, C.C.; Liu, H.H. The empirical mode decomposition and the Hilbert spectrum for nonlinear and non-stationary time series analysis. *Proc. R. Soc. Lond. A Math. Phys. Eng. Sci.* **1998**, *454*, 903–995. [CrossRef]
23. Huang, N.; Shen, Z.; Long, S.R. A new view of nonlinear water waves: The Hilbert spectrum. *Annu. Rev. Fluid Mech.* **1999**, *31*, 417–457. [CrossRef]
24. Huang, N.; Wu, M.L.; Qu, W.; Long, S.; Shen, S. Applications of Hilbert–Huang transform to non-stationary financial time series analysis applied stochastic models in business and industry. *Appl. Stoch. Models Bus. Ind.* **2003**, *19*, 245–268. [CrossRef]
25. Yu, M.; Erlei, Y.; Bin, R.; Haiyang, Z.; Xiaohong, L. Improved Hilbert spectral representation method and its application to seismic analysis of shield tunnel subjected to spatially correlated ground motions. *Soil Dyn. Earthq. Eng.* **2018**, *111*, 119–130.
26. Zhang, R.R.; Ma, S.; Safak, E.; Hartzell, S. Hilbert–Huang transform analysis of dynamic and earthquake motion recordings. *ASCE J. Eng. Mech.* **2003**, *129*, 861–875. [CrossRef]

27. Park, Y.J.; Ang, A.H.-S. Mechanistic seismic damage model for reinforced concrete. *J. Struct. Eng.* **1985**, *111*, 722–739. [CrossRef]
28. Park, Y.J.; Ang, A.H.-S.; Wen, Y.K. Damage-limiting aseismic design of buildings. *Earthq. Spectra* **1987**, *3*, 1–26. [CrossRef]
29. Kunnath, S.K.; Reinhorn, A.M.; Abel, J.F. A Computational Tool for Seismic Performance of Reinforced Concrete Building. *Comput. Struct.* **1992**, *41*, 157–173. [CrossRef]
30. Kunnath, S.K.; Reinhorn, A.M.; Lobo, R.F. *IDARC Version 3.0: A Program for the Inelastic Damage Analysis of Reinforced Concrete Structures, Report No. NCEER-92-0022*; National Center for Earthquake Engineering Research; University at Buffalo: Buffalo, NY, USA, 1992.
31. Eurocode 8. *Design of Structures for Earthquake Resistance—Part 1: General Rules, Seismic Actions, and Rules for Buildings*; European Committee for Standardization: Brussels, Belgium, 2004.
32. Eurocode 2. *Design of Concrete Structures—Part 1: General Rules and Rules for Building*; European Committee for Standardization: Brussels, Belgium, 2000.
33. Reinhorn, A.M.; Roh, H.; Sivaselvan, M.; Kunnath, S.K.; Valles, R.E.; Madan, A.; Li, C.; Lobo, R.; Park, Y.J. *IDARC2D Version 7.0: A Pprogram for the Inelastic Damage Analysis of Structures*; Tech. Rep. MCEER-09-0006; MCEER, State University of New York at Buffalo: Buffalo, NY, USA, 2009.
34. Gholamreza, G.A.; Elham, R. Maximum damage prediction for regular reinforced concrete frames under consecutive earthquakes. *Earthq. Struct.* **2018**, *14*, 129–142.
35. The Math Works Inc. *MATLAB and Statistics Toolbox Release 2016b*; The Math Works Inc.: Natick, MA, USA, 2016.